Journal of the Geological Society, London, Vol. **157,** 2000, pp. 795–809. Printed in Great Britain.

U–Pb and $^{40}Ar/^{39}Ar$ constraints on the Fjord Region Detachment Zone: a long-lived extensional fault in the central East Greenland Caledonides

E. H. HARTZ[1], A. ANDRESEN[1], M. W. MARTIN[2] & K. V. HODGES[2]

[1]*Department of Geology, PO Box 1047, University of Oslo, N0316 Oslo, Norway (e-mail: ebbe.hartz@geologi.uio.no)*

[2]*Department of Earth, Atmospheric, and Planetary Sciences, Massachusetts Institute of Technology, Cambridge, USA*

Abstract: The high strain zone separating infracrustal ortho- and paragneisses from supracrustal cover rocks in the East Greenland Caledonides has been interpreted variously as (1) a combined Grenvillian and Caledonian thrust, (2) a Vendian extensional shear zone reactivated as a Caledonian thrust, (3) a Caledonian extensional detachment reactivated as a late Caledonian thrust or (4) a late Caledonian extensional detachment. In this study we present new kinematic and geochronological data (U–Pb and $^{40}Ar/^{39}Ar$) from a well-studied segment of the high strain zone in Kejser Franz Joseph Fjord, demonstrating top-to-the-east, normal-sense displacement. Syntectonic peraluminous granites in the infrastructure are interpreted to have formed by decompressional anatexis (*c.* 430–425 Ma) and were later deformed to ultramylonites, cataclasites and psudotachylites along the high strain zone. Extension related fabrics overprint earlier and are synchronous with contractional top-to-the-NW thrust faults and associated structures. Muscovite records progressively younger $^{40}Ar/^{39}Ar$ cooling ages (from 408 to 388 Ma) downward in the extensional footwall, whereas feldspar from the mylonites yield a closure age of 349 Ma. Foreland-directed shortening in the East Greenland Caledonides lasted until at least Early Devonian times, while orogenic extensional collapse initiated along the zone of high strain during the Late Silurian in an overall collisional setting. Upper crustal thinning continued well into the Devonian along increasingly more narrow and brittle extensional faults.

Keywords: extension, Caledonides, Greenland, $^{40}Ar/^{39}Ar$, U–Pb.

Since recognition of syn-collisional collapse structures in the Himalayas (Burg *et al.* 1984; Burchfiel & Royden 1985), similar relationships have been recognized in many orogens, including the Scandinavian Caledonides (e.g. Andersen 1993). In the East Greenland Caledonides, a recently discovered extensional detachment separates high-grade ortho- and paragneisses in the footwall from Late Proterozoic sedimentary rocks, mostly of low metamorphic grade in the hanging wall (Soper & Higgins 1993; Strachan 1994; Hartz & Andresen 1995; Fig. 1). However, tectonic models presented to explain these structures have varied considerably, reflecting the lack of both detailed kinematic data and reliable geochronological data.

Rocks of the East Greenland Caledonides are divided into four major lithotectonic units (Fig. 1a and b): (1) Archean to Early Proterozoic continental rocks of the Laurentian shield covered by Mid-Proterozoic supracrustal rocks (Henriksen 1985); (2) a *c.* 17 km thick sequence of Late Proterozoic (the Eleonore Bay Supergroup) to Middle Ordovician, mostly shallow-marine sedimentary rocks (Fränkl 1956; Sønderholm & Tirsgaard 1993); (3) large volumes of Silurian to Devonian intrusive rocks (Haller 1971); (4) continental clastic and volcanic deposits of Devonian (Nathorst 1901). In addition, the Caledonian rocks are overlain by a thick sequence of Carboniferous to Tertiary sedimentary and volcanic rocks along the coastal areas of central East Greenland (Koch & Haller 1971).

The age and origin of the high strain zone at the base of the Eleonore Bay Supergroup has been debated in the literature for almost 70 years. First recognized and described in the Kejser Franz Joseph Fjord, it was interpreted as a thrust fault, with top-to-the-west displacement of the sedimentary rocks in the hanging wall (Whittard 1930) (Fig. 2a). Subsequently, Wegmann (1935) (Fig. 2b) reinterpreted the structure as a sharp metamorphic front within the framework of a 'mobile infrastructure'. Haller (1955, 1971) suggested that the supracrustal rocks slid off the rising migmatite domes along an extensional 'zone of disharmonic detachment', coinciding with the metamorphic front (Fig. 2b).

On the basis of studies during the 1970s, the high strain zone at the base of the Eleonore Bay Supergroup was reinterpreted as a thrust fault (Higgins 1976; Rex *et al.* 1977; Henriksen 1985; Rex & Higgins 1985) (Fig. 2c). These authors concluded that the fold structures in the footwall gneisses were predominantly of pre-Caledonian age. This interpretation was strongly influenced by (1) Precambrian Rb–Sr (whole rock and mineral isochrons) and U–Pb zircon ages derived from granites and metamorphic rocks in the core complex (i.e., if late tectonic granites are Grenvillian then the deformation must be at least this old) and (2) intense deformation and metamorphism recorded in the footwall gneisses was not evident in the overlying Late Proterozoic Eleonore Bay Supergroup therefore the central metamorphic complex was inferred to be only weakly 'Caledonized'. Larsen & Bengaard (1991) also interpreted the lower boundary of the Eleonore Bay Supergroup to be a system of thrust faults, but of composite Grenvillian and Caledonian age, cut by steep oblique left lateral normal faults (Fig. 2d).

Soper & Higgins (1993) interpreted the high strain zone as a Vendian extensional detachment fault developed during the initial rifting that led to the opening of the Iapetus ocean, and inferred that the detachment later was reactivated as a Caledonian thrust (Fig. 2e). Strachan (1994), Friderichsen *et al.* (1994), and Dallmeyer *et al.* (1994) concluded that the lower boundary of the Eleonore Bay Supergroup at Ardencaple Fjord (Fig. 1) was a Late Silurian to Early

Devonian extensional detachment fault, reactivated as an Early Devonian thrust (Fig. 2f). More recently, Hartz & Andresen (1995) suggested that high strain zones at the base of the Eleonore Bay Supergroup are late Caledonian detachments (Fig. 2g), and that displacement along these is associated with the development of post-Caledonian/Devonian supradetachment basins. This interpretation was strongly opposed by Leslie & Higgins (1998), who interpret the base of the Eleonore Bay Supergroup as 'a broad top-to-the northwest shear zone, lacking true mylonites', and comment that 'there is little evidence within this region to support the crustal-scale extension invoked in some recent papers (e.g., Hartz & Andresen 1995) to explain major features of the East Greenland Caledonides'. Leslie & Higgins (1998) further argue that the granites intruding metasediments in the area are both Grenvillian and Caledonian in age, based on earlier Rb–Sr dating done in the early 1980s (Rex & Gledhill 1981). Accordingly, they refer to the area between their Rendalen thrust and the Eleonore Bay Supergroup (Fig. 2) as the 'Grenville triangle'.

All previous studies have placed the base of the upper plate at the Junctiondal fault (Fig. 3; Haller 1971), a late brittle fault dipping 70° toward ESE with dip-slip lineations. The fault (and other minor subparallel brittle faults near Junctiondal) cuts the gently east-dipping gneisses and juxtaposes rocks of similar appearance. We follow conclusions of Hartz & Andresen (1995) and place the upper plate-lower plate boundary farther to the east, at the fault separating high-grade rocks of the footwall from low-grade rocks of the hanging wall (Figs 3, 4a).

Andresen *et al.* (1998) infer that the detachment zone can be traced from Scoresby Sund northwards to Ardencaple Fjord (Fig. 1), and named it the Fjord Region Detachment Zone. Peak metamorphic conditions in the lower plate gneisses of Kempes Fjord (Fig. 1) reached at least 1 to 1.2 GPa and 700–850°C, and were subsequently exhumed to *c.* 0.35 GPa at 650°C (Vold 1997; Andresen *et al.* 1998). Vold (1997) relates this pressure–temperature (*P–T*) evolution to Caledonian processes. Caledonian eclogites and garnet websterites record ultra-high-pressure metamorphism (2.35 GPa and 700–800°C) in northern East Greenland (Brueckner *et al.* 1998), suggesting that at least some parts of the Laurentian crust now exposed in East Greenland was extremely overthickened during the Caledonian orogeny. $^{40}Ar/^{39}Ar$ ages from Hudson Land (Fig. 1) document that extension in the hanging wall of the Fjord Region Detachment Zone began before *c.* 422 Ma, based on crystallization ages of lamprophyre dikes that intrude normal faults (Andresen *et al.* 1995; Hartz 1998). These authors also report $^{40}Ar/^{39}Ar$ ages for muscovite and biotite and feldspar from basement gneisses that range from Early Devonian to Carboniferous, which they relate to extensional exhumation of fault-blocks.

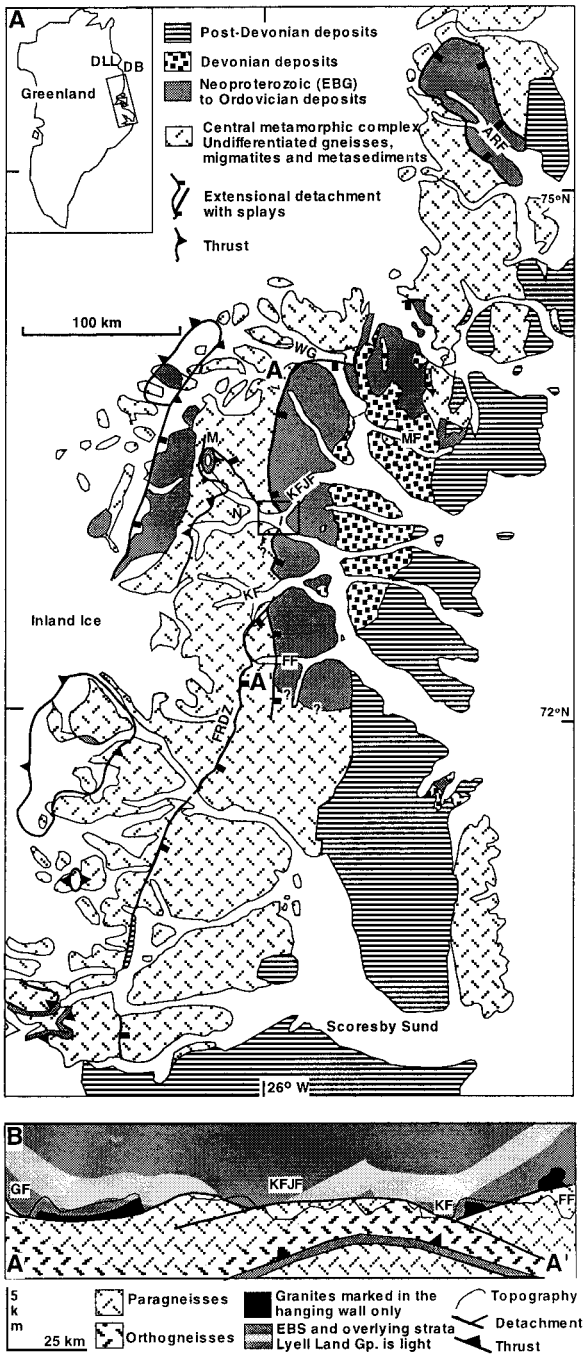

Fig. 1. (**a**) Simplified geological map of East Greenland showing the relationship between Archaean and Proterozoic infracrustal rocks and overlying Neoproterozoic to Middle Ordovician supracrustal rocks. The age of the metasediments is subject of continues research. Also shown are the Devonian molasse and younger deposits. Continuation of the Fjord Region Detachment Zone (FRDZ) north of Kejser Franz Joseph Fjord (KFJF) and south of Forsblad Fjord (FF) is speculative. Possible splays of the detachment are marked as thin lines. The studied area is framed. Other abbreviations: AF, Alpefjord; ARF, Ardencaple Fjord; DB, Dove Bugt; DLL, Dronning Louis Land; GF, Geologfjord; HL, Hudson Land; KF, Kempes Fjord; MF, Moskusoksefjord; Må, Målebjerg; NS, Niggli Spids; A-A′ marks extent of profile in (b). The map is based on Koch & Haller (1971), Henriksen (1985), Escher & Jones (1998), Leslie & Higgins (1998) and our own studies. (**b**) Schematic profile following 26°W longitude (A-A′ marked on a). The extent of ortho- and paragneisses below the Fjord Region Detachment Zone is speculative. The Lyell Land Gp in the central Eleonore Bay Supergroup is used to illustrate variations in stratigraphic separation across the Fjord Region Detachment Zone along strike. Notice that considerably more of the tectonostratigraphy is cut out by the Fjord Region Detachment Zone in the central section of the profile (both above and below the Fjord Region Detachment Zone). Apparent undulations in the Fjord Region Detachment Zone reflect variations in strike as well as in dip.

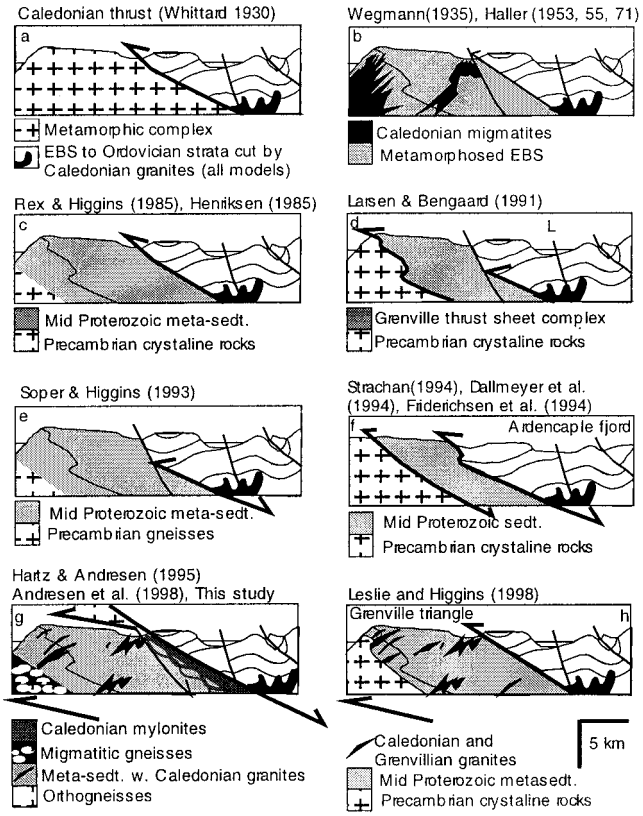

Fig. 2. Eight profiles showing tectonic models for the infracrustal/supracrustal contact in the East Greenland Caledonides, viewed towards North. Models include: (**a**) a Caledonian thrust, (**b**) a Caledonian metamorphic front, (**c**) Caledonian thrusting, (**d**) Grenvillian and Caledonian thrusts, partly cut by Devonian normal faults (L, left lateral fault), (**e**) a Vendian detachment partly reactivated as a Caledonian thrust, and locally cut by post-Caledonian faults, (**f**) a Caledonian detachment reactivated as an Early Devonian thrust, (**g**) a Caledonian to post-Caledonian extensional detachment cutting thrust faults (this study) and (**h**) a Caledonian thrust above the 'Grenville triangle', Model (f) is based on the Ardencaple Fjord area. The other models are based on the studied profile in Kejser Franz Joseph Fjord. Notice that we (g) have moved the contact 2 km eastwards and to a higher position the tectonostratigraphy. The orthogneiss thrust sheet, placed above the profile is located on the southern side of the fjord.

The regional high-strain zone juxtaposing lower and upper crustal rocks plays a key role in our interpretation of the East Greenland Caledonide evolution. Here, we present new kinematic data from a transect across the high-strain zone into the granite-intruded metasediments of the carapace of the Niggli Spids Migmatite Dome. In addition, new U–Pb ages and $^{40}Ar/^{39}Ar$ cooling ages are presented for mylonites and syn-kinematic peraluminous granites exposed in the upper part of the footwall (Fig. 3). These data supports a model that requires significant crustal unroofing along a ductile extensional detachment system during late Silurian time with brittle reactivation at upper crustal levels through the Devonian.

Kinematic evolution of the Fjord Region Detachment Zone in Kejser Franz Joseph Fjord

The rocks along the studied traverse in the Kejser Franz Joseph Fjord region can be divided into three structural units: (1) the structurally lowest comprises parauthocthonous Late Proterozoic (Eleonore Bay Supergroup) to Ordovician deposits that rest depositionally on a pre-Eleonore Bay Supergroup basement and are overthrust by (2) high-grade ortho and paragneisses (Haller 1953; Leslie & Higgins 1998; Escher & Jones 1998). (3) The highest structural unit consists of allochthonous low grade Eleonore Bay Supergroup and younger sediments occuring structurally above these high-grade nappes. The contact separating the two lower structural units is a highly strained unconformity towards the west (Andresen *et al.* 1998). The contact separating the two upper structural units (the base of the Eleonore Bay Supergroup) is the extensional detachment (the Fjord Region Detachment Zone) (Hartz & Andresen 1995), described in this paper. The detachment zone involves four structural domains: (1) the Niggli Spids Migmatite Dome and its metasedimentary carapace (Haller 1953), which crops out from Niggli Spids, along Kap Lapparent to Junctiondal (Fig. 3); (2) the high-strain mylonitic front that defines the detachment zone structurally below the carapace; (3) a late brittle detachment fault which overprints ductile structures along the uppermost detachment zone; and (4) the hanging wall above the Late Brittle Detachment Fault, consisting of relatively low-grade sediments intruded by leucogranites.

Niggli Spids Migmatite Dome

The Niggli Spids Migmatite Dome has been described as a more than 1 km thick sequence of megacrystic augen orthogneisses, cut by a net of leucogranites, which is capped by metasediments (quartzite, gneisses, schists and marbles) (Haller 1953; Escher & Jones 1998). However, the localities we visited during a reconnaissance trip by boat to the base of the otherwise inaccessible 2 km high cliff at Niggli Spids, show that deformed granitic veins cut both the migmatitic gneisses and overlying metasediments (Fig. 4b). Although these gneisses in the core of the dome are highly migmatitic (>50% variably deformed leucosome) continuous bands in the gneisses along the entire wall can be visually distinguished (Fig. 4b). The concentration of leucosome gradually decreases upwards, where the granites are concentrated in veins cutting the paragneisses, as at Kap Laparent (Fig. 4d). K-feldspar, biotite augen gneisses occur above the Niggli Spids Migmatite Dome in the high cliffs on the south side of Kejser Franz Joseph Fjord (Figs 1 and 2). These are inferred to be orthogneisses thrust over the Niggli Spids Migmatite Dome; however, the actual thrust was not located.

At Kap Lapparent (Fig. 1) the carapace of the Niggli Spids Migmatite Dome comprises quartzose metasediments and coarse-grained kyanite–silliminite–garnet muscovite and biotite gneisses (Fig. 4e). These supracrustal rocks are intruded by dolerite dykes that have been deformed and metamorphosed together with the country rock (Haller 1971). Peak metamorphic conditions are comparable to those estimated by Vold (1997) for the Kempes Fjord area (discussed previously) (Fig. 1).

It has been argued that these metasediments are either Late Proterozoic (middle section of Eleonore Bay Supergroup (Haller 1953) or Mid-Proterozic in age (e.g. Henriksen, 1985; Leslie & Higgins 1998) (Fig. 2). However, the sedimentary units characteristic of the middle part of the Eleonore Bay Supergroup, have not been recognized below the Fjord Region Detachment Zone in Kejser Franz Joseph Fjord. Therefore,

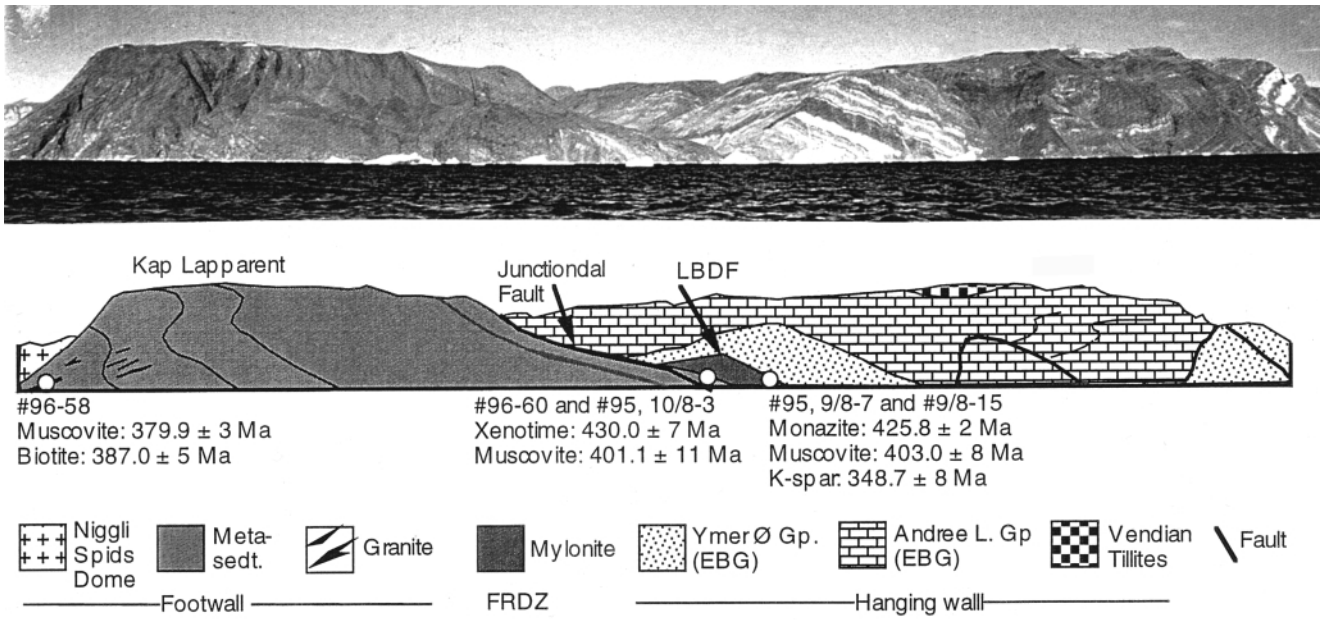

Fig. 3. (**a**) View to the North of the studied transect. The Fjord Region Detachment Zone (FRDZ) is defined by the zone of mylonite. The Late Brittle Detachment Fault (LBDF) dips as a sharp plane 30° down towards East, juxtaposing the Late Proterozoic Ymer Ø and Andree Land Group of the Eleonore Bay Supergroup, and Vendian tillites in the upper plate, against gneisses, metasediments and migmatites in the lower plate. Field of view 23 km. The wall at Kap Lapparent is 1.5 km high. Notice that we, in contrast to earlier workers, extend the lower plate eastwards of the Junctiondal Fault. Isotopic data for each site is included. Ar data (muscovite and biotite) are combined as error-weighted mean. U–Pb data (monazite and xenotime) are upper intersects. See tables for details. (**b**) Northwards view of the upper plate. Note that the carbonate beds are cut by steep faults. The faults are inaccessible, but are estimated to dip steeply (*c.* 80°) towards west. In their current position are these therefore reverse faults. However, the faults extend bedding. We thus tentatively suggest that the faults are rotated with bedding due post-extensional folding.

the sediments are either lower Eleonore Bay Supergroup or older. We speculate that the quartzitic gneisses, marbles and amphibolite-grade mafic dykes at Niggli Spids Migmatite Dome and Kap Lapparent may be the metamorphic equivalents of quartzites, carbonates and lamprophyre dykes of the low-grade lower Eleonore Bay Supergroup observed elsewhere (e.g. Fränkl 1956). Haller (1970) identified two generations of major (>1 km amplitude) folds in the Niggli Spids Migmatite Dome, both of which occur within the Kejser Franz Joseph Fjord structural section. The first generation (F_1) trend subparallel to the shallowly east- to SE-plunging stretching lineation defined by elongated feldspars and aligned micas (Figs 4f and 5a). These folds are predominantly open to closed and sub-cylindrical. Axial planes of the F_1 folds are often subparallel to the foliation, and the vergence towards North. The F_1 folds only occur below the Fjord Region Detachment Zone, and are interpreted to have formed synchronously with peak metamorphism.

Quartz+feldspar layers in the gneisses, as well as some of the peraluminous granitic veins, are boudinaged. The necklines of the boudins typically plunge gently north to NE (Figs 4g and 5b). The boudins commonly are asymmetric, consistent with top-to-the-east extensional shear. The early D_1 structures have been refolded by NNE-trending F_2 folds. F_2 folds are overturned to recumbent and generally plunging towards NNE. Hinges of F_2 folds are generally straight, however, curved hinges and sheath folds occur locally, particularly in the upper part of the detachment zone. In the lower section of the transect, from Kap Lapparent to Junctiondal (Fig. 3) F_2 folds verge towards both NW and east. Towards structural higher levels F_2 folds consistently verge towards east or SE (Figs 4h and 5c).

Peraluminous granitic veins probably developed by anatexis in the core of Niggli Spids Migmatite Dome are segregated into veins that cut the foliation at higher structural levels. However also above the core of Niggli Spids Migmatite Dome as in Junctiondal, does the peraluminous granitites develop *in situ* as millimetre to decimetre-thick veins (Figs 4f and h). These granitic veins cut F_1 folds and either predate or are synchronous with the F_2 folds (Fig. 4f). Where the granitic veins are deformed by F_2 folds, a weak axial planar cleavage defined by muscovite is developed. Some of the granitic veins cut through F_2 folds along their axial planes, as observed both at Junctiondal (Fig. 4h) and at Kap Lapparent, where kilometre-scale east-vergent F_2 folds are cut by granitic veins that intrude along axial planes (Fig. 4d).

Fig. 4. Structures in the lower (western) section of the profile. The view is northwards in all photos, except (b) and (c), which are viewed towards west. (**a**) The Fjord Region Detachment Zone. The top of the detachment extends as a sharp plane below the pale grey carbonates (just left of the iceberg). Notice the top-to-the-west F_2 folds in the hanging wall. The wall is 1300 m high. (**b**) Niggli Spids: migmatitic orthogneisses and overlying (darker) anatectic paragneisses. The wall is *c.* 2 km high. (**c**) Migmatitic gneisses in the core of the Nigg;i Spids Migmatite Dome. (**d**) F_2 folds at Kap Lapparent. Notice that the 20 m thick lecogranitic veins follow the axial planes. (**e**) Folded metasediments, at the base of Kap Lapparent. (**f**) F_1 fold in Junctiondal. The axis of the fold plunges towards ESE. The F_1 folds are cut by granitic veins. (**g**) Boudinaged granites in Junctiondal formed by east–west extension, and later deformed by east-verging F_2 folds. (**h**) Granitic veins in Junctiondal are typically folded by the F_2 folds; however, some late veins cut across these (helmet for scale at top of photo).

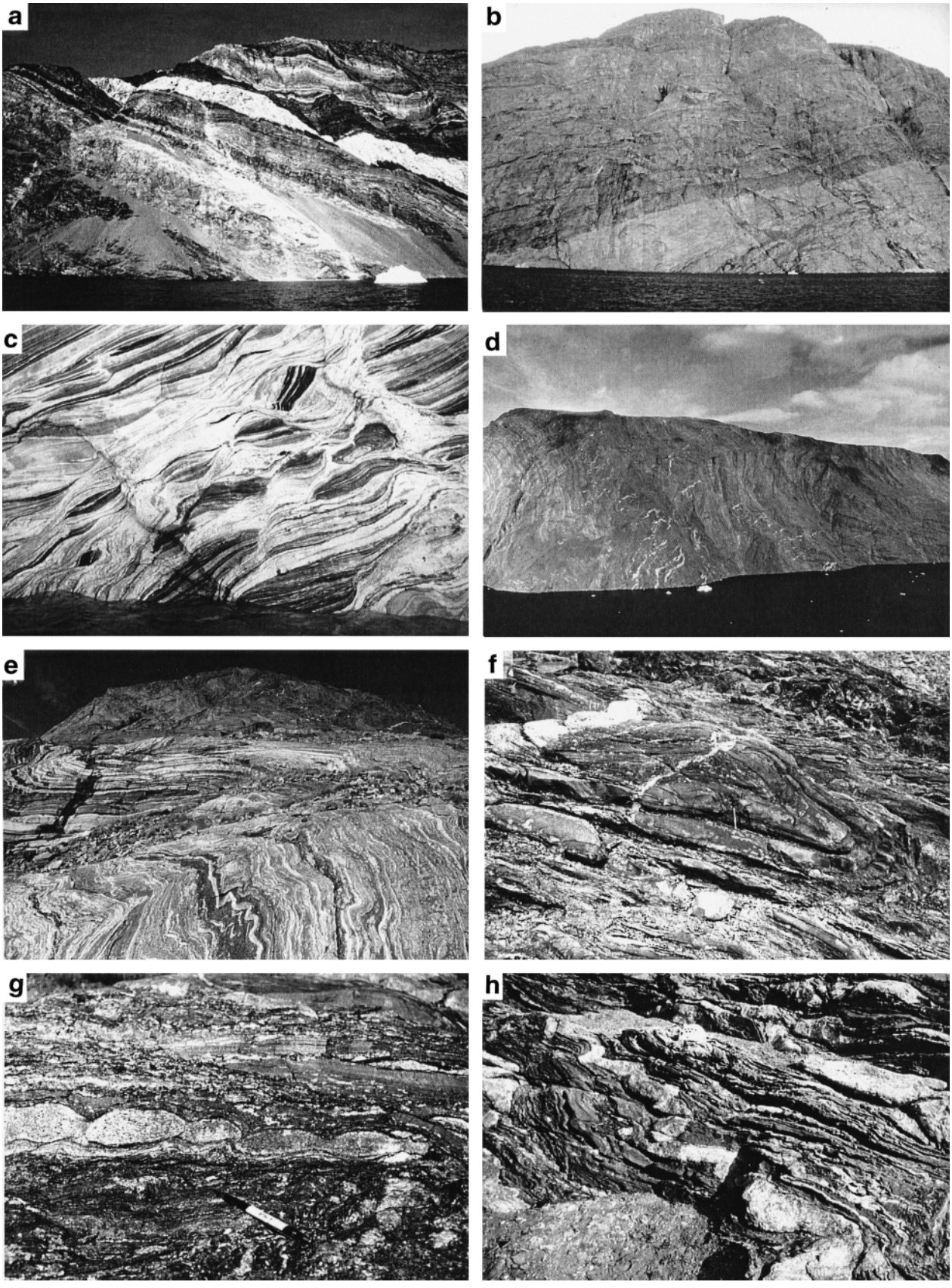
a
b
c
d
e
f
g
h

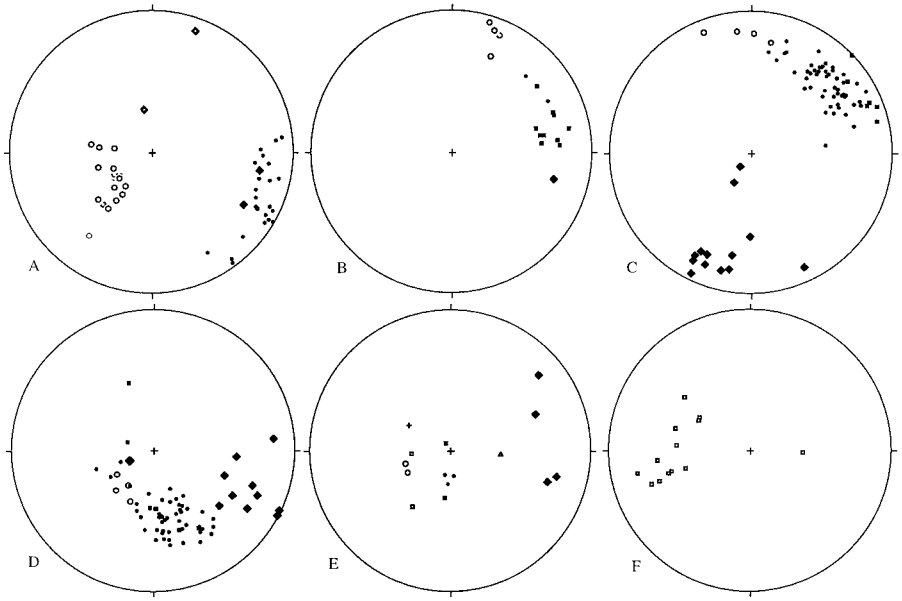

Fig. 5. Stereonets (lower hemisphere, equal area) showing (**a**) F_1 folds from Junctiondal (axes are filled circles; axial planes are open circles), and Kap Lapparent (axes are filled diamonds; axial planes are open diamonds). (**b**) boudin axes (open circles), and associated stretching lineations from Junctiondal (filled circles), Kap Lapparent (diamonds), and the detachment mylonites (squares); (**c**) axis of the F_2 folds at Kap Lapparent (diamonds), Junctiondal (filled circle), the detachment mylonites (open circles) and the Carbonate above the detachment (squares); (**d**) Axial planes of F_2 folds from Kap Lapparent (filled diamonds), Junctiondal (filled circles), top of the detachment (open circles), and carbonates directly above the detachment (filled squares). (**e**) S–C structures from Junctiondal (S, open circle; C, filled circle), the detachment (S, open square; C, filled square), and the carbonate (S, triangle; C, cross). The filled diamonds mark the direction of extension on the S-plane, perpendicular to the S–C intersection lineation. (**f**) Fracture planes in the uppermost brittle part of the detachment zone.

In contrast to the overturned to slightly recumbent style of the F_2 folds, the N–S-trending F_3 folds are typically large wave length, open, upright and symmetrical (Figs 3a and 4b) and can be traced for hundred of km (Haller 1970). Where F_2 and F_3 folds types interfere, are they not always easily distinguishable.

Fjord Region Detachment Zone

East of Junctiondal numerous anastomosing mylonitic extensional shear zones, cut the fabrics typical for Niggli Spids Migmatite Dome. However, lenses with a pre-mylonitic fabric are locally preserved, some of which contain folds with top-to-the-west vergence (Fig. 6a), illustrating that contraction related structures existed prior to the mylonitic extensional structures. The uppermost 300 m of the detachment zone is dominated by zones of mylonitic augen gneiss with a consistent top-to-the-east shear sense (Fig. 6b) and lenses of less deformed leucogranite. Ascending upwards across this detachment zone, the leucogranites gradually become transformed into augen gneisses and mylonites, documenting an upward increase in shear strain. Locally, fine-grained peraluminous granite veins cut the mylonitic fabric, indicating that the granites are syn-kinematic. The upper part of the detachment zone is dominated by banded mylonites composed of 1–10 cm thick layers of alternating coarse mica- and feldspar-rich layers (Fig. 6c). Muscovite porphyroclasts are folded or deformed into sigmoidal mica fish (Fig. 6d). Feldspars are ductilely deformed into asymmetric augen with pressure shadows (Fig. 6e). Kinematic indicators, including asymmetric F_2 folds (Figs 5c, d and 6b), sigmoidal mica fish, lineations, extensional shear bands, S–C structures (Berthé *et al.* 1979) (Fig. 5d), and normal slip crenulations (Dennis & Secor 1987) (Fig. 6d) all indicate consistent top-to-the-east extensional sense of shear. The banded mylonites grade upward into homogeneous ultramylonite which characterize the uppermost 10 m of the detachment zone.

Late Brittle Detachment Fault

The Late Brittle Detachment Fault consists of laterally continuous cataclasite zones up to 0.5 m, but typically less than 10 cm thick. They occur from Junctiondal eastward and become more numerous toward the top of the detachment

Fig. 6. Structures in the Fjord Region Detachment Zone; all are viewed towards the north, except (d) and (e), which are viewed towards south. (**a**) Boudinaged lense with west-verging folds, surrounded by mylonites with east-verging folds (seen above the lense). Height of photo is 1 m. (**b**) Sharp transition between a weakly and strongly foliated augen gneiss. Notice the sigmoidal shape of augens and extensional shear bands, all of which show a down-towards east sense of shear. Rocks surrounding this body are highly strained mylonites as shown in (c). (**c**) Mylonites to ultramylonites *c.* 14 m below the top of the detachment. Vergence of the F_2 folds is towards the east. (**d**) Muscovite-rich layers show a pronounced asymmetry, with penetrative extensional down-to-the east shear bands. Length of photo is 3.5 mm. (**e**) The same rock as in (c) viewed in thin section. Bands with considerable grain size reduction alternate with less fine-grained mylonites. Notice the sigmoidal feldspar augen again shows top-towards-east sense of shear. Height of photo 7 mm. (**f**) Mylonites 5 m into the detachment zone are strongly brecciated. (**g**) Brecciated pseudotachylite forming the uppermost metre in the detachment zone. (**i**) Sigmoidal structures in the carbonate directly above the detachment show consistent eastwards shearing.

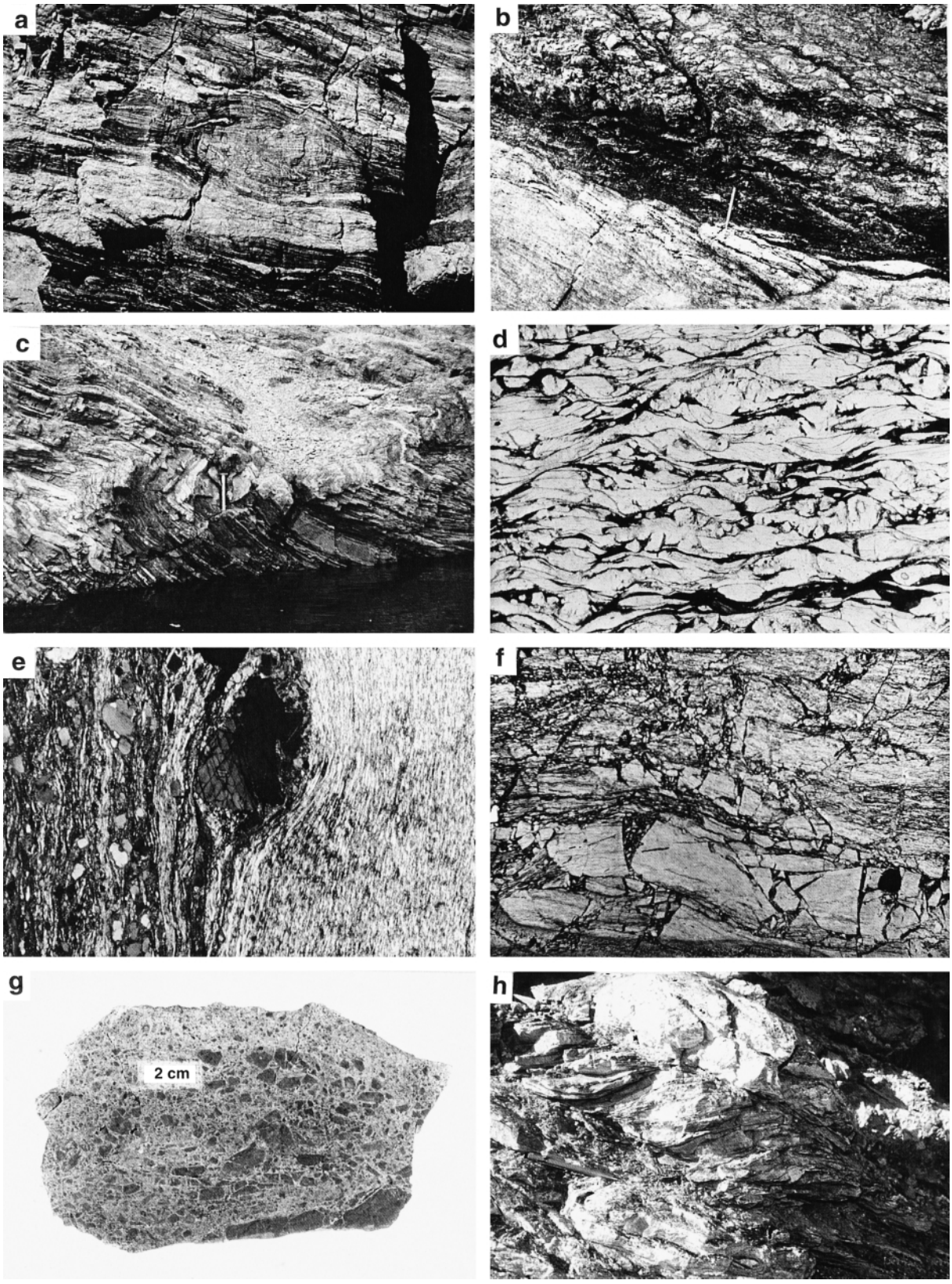
a
b
c
d
e
f
g
2 cm
h

zone. In the interval from 7 to 5 m below the Late Brittle Detachment Fault, there is a gradual transition upwards from mylonite to cataclasite and ultracataclasites (Figs 5f, 6f). Breccia clasts in the cataclasites show evidence for multiple phases of brecciation. The uppermost 2.5 m of the detachment zone consists of pale grey, pseudotachylyte (Fig. 6g), which in the uppermost meter of the detachment zone is intensely brecciated. Three laterally extensive 10 cm thick zones of dark grey, glassy pseudotachlyte cut these upper cataclasites, demonstrating that brecciation and formation of pseudotachylytes alternated in time and space.

Hanging wall block

The hanging wall of the Fjord Region Detachment Zone comprises low-grade shallow marine sediments of the Eleonore Bay Supergroup, Vendian tillites, Cambrian shales and sandstones, and Ordovician carbonates. If the metasediments below the detachment in Kejser Franz Joseph Fjord are of Mid-Proterozoic age has the lowermost 14 km of the Eleonore Bay Supergroup occurring elsewhere below the Ymer Ø and Andree Land Groups (Sønderholm & Tirsgaard 1993) has been cut out by the Fjord Region Detachment Zone (Figs 1b and 3). Regardless of the stratigraphic age of the metasediments below the detachment, there is a major metamorphic break across the detachment zone to the upper amphibolite-grade gneisses below. The two-mica granites present in the shear zone do not intrude the hanging wall of the detachment in Kejser Franz Joseph Fjord, but are common in the lower part the hanging wall farther to the north (Koch & Haller 1971).

Rocks forming the lowermost 10 m of the hanging wall also contain top-to-the-east structures. Open to close, east-verging, F_2 folds occur in the carbonates directly above the detachment, as do east-dipping duplexes and S–C fabrics indicative of top-to-the-east extensional displacement (Fig. 6h). Structurally higher (*c*. 200 m) in the hanging wall, west-verging folds and minor top-to-the-west thrusts are common (Figs 3 and 4a). The hanging wall is also cut by numerous planar brittle extensional faults, some of which cut folds. In some locations can it be demonstrated that F_3 folds postdate the extensional faults. Typically is bedding cut by extensional faults with an angle of 60 to 70°, but as F_3 folds rotate bedding does faults rotate across vertical into an apparent reverse fault geometry (Fig. 3). Similar major north–south trending F_3 folds and parallel thrust faults also occur in the collapse basins of Devono-Carboniferous age farther east (Koch & Haller 1971), again suggesting that at least in part does the F_3 folds postdate the Silurian to Devonian extensional collapse.

Geochronology

In order to constrain the timing of igneous activity, the timing of deformation of the Fjord Region Detachment Zone, and the exhumation history of the footwall, samples were collected from key localities both from within and below the detachment zone, and were dated using both U–Pb and $^{40}Ar/^{39}Ar$ methods.

Isotopic results and their significance

Five samples were collected for $^{40}Ar/^{39}Ar$ and U–Pb dating to obtain information on the tectonic history of the Fjord Region Detachment Zone. Two of the analysed samples are from granitic mylonites in the uppermost part of the footwall directly beneath the detachment (9/8-7 and 9/8-15), two are from veins of leucogranite at Junctiondal (96-60) and Kap Lapparent (96-58), and one sample is of gneiss at Junctiondal (10/8-3). Isotopic results and analytical methods are listed in Table 1 (U–Pb) and Table 2 ($^{40}Ar/^{39}Ar$).

Mylonites from the upper detachment zone. Two samples of the mylonitic granite in the upper part of the detachment zone were collected from 7 m (95, 9/8-7) and 15 m (95, 9/8-15) structurally below the Late Brittle Detachment Fault. Six monazite crystals from sample 95, 9/8-7 were analysed and are normally discordant. The analyses define a linear array with an upper intercept of 425.8 ± 2.0 Ma (MSWD = 0.08). The U–Pb systematics of these monazites are distinct from other monazite U–Pb behavior from undeformed or mildly deformed Caledonian leucogranites of the same age in the same region (Hartz *et al*. in press) or such as sample sample #60 discussed below. We attribute the systematic normal discordancy displayed by these monazites to be related to the affects of the high strain state experienced by this sample during the formation of mylonitic fabric along the extensional detachment and therefore we interpret this age as a minimum age of the leucogranite. However, given the field relationships and the variation of nondeformed to strongly deformed Caledonian leucogranites in the region, we do interpret this to be a Caledonian intrusion.

UV-laser spot fusion $^{40}Ar/^{39}Ar$ dates from a single large muscovite grain yielded a weighted mean of 408.0 ± 6.2 Ma (Fig. 7b). This date is indistinguishable from an inverse isochron date of 408.7 ± 6.5 Ma (Fig. 7b), obtained by *in situ* UV and Ar-ion laser spot analyses of a second large muscovite in a thin section (Fig. 8a–c). The spot dates show some intragranular variations, with the dates ranging from as old as *c*. 423 Ma to as young as *c*. 390 Ma. The distribution of these dates have no obvious trend with position in the crystals (Fig. 8d) (e.g. the youngest ages did not cluster near the rims), so we regard the variation as neither a slow cooling phenomenon (Hodges & Bowring 1995) nor a problem of excess ^{40}Ar (Onstott *et al*. 1991). Because the muscovite is deformed (Figs 6d, 8d), it may indicate late, deformation-induced ^{40}Ar loss. Another smaller muscovite crystal in the thin section was dated at *c*. 404 Ma. This date is indistinguishable from the mean fusion age obtained by total fusion of nine small muscovites grains (404.1 ± 8.6 Ma) (Table 2). Again, a range of dates was obtained, in this case varying from *c*. 425 Ma to *c*. 381 Ma. Small muscovite grains from sample 95, 9/8-15 yielded a weighted mean date of *c*. 400.0 ± 3.0 Ma. K-feldspar in the thin section was dated by UV and Ar-ion laser spot fusion (Fig. 8e and f), yielding collectively a weighted mean date of *c*. 348.7 ± 8.1 Ma (Figs 7b and 8d).

Peraluminous granitic veins cutting gneiss at Junctional. Peraluminous granitic veins cut the amphibolite-facies metamorphic foliation and the related F_1 folds at Junctiondal. The sampled 30 cm thick dyke (96-60) is weakly deformed and intrudes across F_2 folds in the gneiss, but is also folded into an east-verging F_2 fold, which we interpret as syntectonic with F_2 deformation (Fig. 6h). An age of this sample will therefore constrain late-post high grade metamorphism and deformation in the area. Zircon, monazite, xenotime and white mica were extracted from the sample.

A single clear, euhedral zircon crystal gave a discordant $^{207}Pb/^{206}Pb$ date of 1209 Ma, which we interpreted to be

Table 1. *U–Pb isotopic data for zircon, monazite, and xenotime from Kejser Franz Fjord, East Greenland*

Fractions[a]	Weight (μg)	Concentration (ppm)				Error (2 sigma %)						Age (Ma)			Corr. coef.	Pb (pg)[e]
		U	Pb	$^{206}Pb/^{204}Pb$[c]	$^{208}Pb/^{206}Pb$[d]	$^{206}Pb/^{238}U$[d]	Error	$^{207}Pb/^{235}U$[d]	Error	$^{207}Pb/^{206}Pb$[d]	Error	$^{206}Pb/^{238}U$	$^{207}Pb/^{235}U$	$^{207}Pb/^{206}Pb$		
95,9/8-7																
m1	0.7	5117.6	936.3	339.8	1.850	0.06796	(0.12)	0.51839	(0.20)	0.05533	(0.15)	*423.8*	*424.1*	*425.5*	0.64	47.5
m2	0.4	7085.6	1149.4	1356.1	1.721	0.06680	(0.16)	0.50951	(0.27)	0.05532	(0.21)	*416.9*	*418.1*	*425.0*	0.63	9.0
m3	0.4	9513.3	1831.1	255.9	2.001	0.06651	(0.13)	0.50703	(0.34)	0.05529	(0.30)	*415.1*	*416.5*	*423.9*	0.47	71.8
m4	0.7	9606.9	1779.1	448.5	2.018	0.06624	(0.08)	0.50523	(0.13)	0.05532	(0.10)	*413.5*	*415.2*	*425.1*	0.66	68.6
m5	0.5	5607.8	970.1	279.6	1.738	0.06560	(0.14)	0.50043	(0.23)	0.05533	(0.18)	*409.6*	*412.0*	*425.6*	0.63	47.7
m6	0.9	15 318.2	2740.8	545.5	2.299	0.05934	(0.11)	0.45192	(0.17)	0.05523	(0.12)	*371.6*	*378.6*	*421.7*	0.70	97.3
96-60																
z1	2.3	667.6	115.3	2926.6	0.085	0.17085	(0.23)	1.89607	(0.25)	0.08049	(0.10)	*1016.8*	*1079.7*	*1209.0*	0.92	5.7
m1	7.0	9174.6	1730.5	374.7	1.920	0.06865	(0.31)	0.52539	(0.39)	0.05550	(0.22)	*428.0*	*428.7*	*432.6*	0.83	779.6
m2	1.2	10 780.0	1479.4	1096.1	1.198	0.06861	(0.06)	0.52263	(0.09)	0.05524	(0.07)	*427.8*	*426.9*	*422.1*	0.66	51.7
m3	0.8	22 908.6	3802.5	459.9	1.589	0.06848	(0.09)	0.52182	(0.14)	0.05527	(0.10)	*427.0*	*426.4*	*423.1*	0.66	182.6
m4	4.0	11 624.8	1758.1	1224.9	1.447	0.06834	(0.09)	0.52009	(0.12)	0.05520	(0.08)	*426.1*	*425.2*	*420.3*	0.79	163.5
x1	5.7	20 242.8	1345.6	1394.2	0.028	0.06807	(0.13)	0.51983	(0.15)	0.05539	(0.06)	*424.5*	*425.0*	*428.0*	0.91	357.8
x2	3.8	16 077.3	1078.3	1155.7	0.030	0.06792	(0.19)	0.51828	(0.21)	0.05534	(0.08)	*423.6*	*424.0*	*426.2*	0.92	228.7
x3	2.6	15 412.4	1004.0	1712.8	0.028	0.06735	(0.23)	0.51359	(0.27)	0.05530	(0.13)	*420.2*	*420.9*	*424.6*	0.87	99.9
m5	6.3	6677.3	1074.3	984.3	1.625	0.06759	(0.21)	0.51387	(0.25)	0.05514	(0.12)	*421.6*	*421.1*	*418.1*	0.88	185.7
x4	1.7	22 363.8	1511.7	744.7	0.030	0.06643	(0.17)	0.50628	(0.22)	0.05527	(0.14)	*414.6*	*415.9*	*423.3*	0.78	218.0
m6	49.5	8423.0	1229.3	359.7	1.359	0.06433	(0.22)	0.48759	(0.26)	0.05497	(0.13)	*401.9*	*403.3*	*411.1*	0.86	4923.5

Mass fractionation correction of 0.12% ± 0.05%/amu and 0.15% ± 0.04%/amu was applied to dynamic faraday-daly analyses and single collector daly analyses, respectively. Total procedural blank for Pb ranged from 0.65 to 5.0 pg and <1.0 pg for U. Age calculations are based on the decay constants of Steiger & Jäger (1977). Common-Pb corrections were calculated by using the model of Stacey & Kramers (1975) and the interpreted age of the sample.

UTM, universal transverse mercator. Corr. coef.=correlation coefficient.

[a]Sample chemistry follows procedures outlined in Hawkins & Bowring 1997.

[b]Sample weights were estimated by using a videomonitor and are known to within 40%.

[c]Values are measured ratio corrected for spike and fractionation only.

[d]Values are corrected for fractionation, spike, blank, and initial common Pb.

[e]Total common-Pb in analyses.

Table 2. *$^{40}Ar/^{39}Ar$ ages from the Kejser Franz Joseph Fjord profile*

Sample	Rock	Location	Method*	Mineral	Age	2σ/SE	No.	Comment
95, 9/8-7	Mylonite	Upper detachment	TLF	Muscovite	404.1	± 8.6	9	Weighted average
			UV LSF	Muscovite	408.0	± 6.2	6	Weighted average
			In situ UV/Ar-ion LSF	Muscovite	408.7	± 6.5	23	Inverse isochron
			In situ UV/Ar-ion LSF	K-feldspar	348.7	± 8.1	7	Weighted average
95, 9/8-15	Mylonite	Upper detachment	TLF	Muscovite	400.0	± 3.0	10	Weighted average
95, 10/8-3	Gneiss	Junctiondal	TLF	Muscovite	397.1	± 2.8	10	Weighted average
96-60	Granite	Junctiondal	Visual LSF	Muscovite	405.1	± 2.7	13	Inverse isochron
96-58	Granite	Kap Lapparent	TLF	Muscovite	380.9	± 4.9	10	Weighted average
			FSH	Biotite	386.9	± 1.5	7	Plateau age
			Visual LSF	Muscovite	378.7	± 5.7	15	Inverse isochron
			Visual LSF	Biotite	390.2	± 8.7	12	Inverse isochron

*TLF, total laser fusion; LSF, laser spot fusion; FSH, furnace step heating.

$^{40}Ar/^{39}Ar$ analyses were performed at MIT on pure mineral separates and double-polished thick sections (200 μm). Both types of samples were encapsulated in an Al-disk shielded with Cd-foil and irradiated with flux monitor MMHb-1 hornblende (520.4 Ma; Samson & Alexander 1987) at the McMaster Nuclear reactor in Hamilton Ontario, Canada. Radiation parameters and J-values for each sample can be obtained from the Society Library or the British Library Document Supply Centre, Boston Spa, Wetherby, West Yorkshire LS23 7BQ, UK as Supplementary Publication No. SUP 18145 (3 pages). We extracted Ar from samples by one of four methods: (1) *in situ* UV-laser ablation; (2) *in situ* Ar-ion laser fusion; (3) total fusion of single grains using a defocused visual laser beam; and (4) incremental heating of mineral separates using a resistance furnace.

General descriptions of these techniques can be found in Hodges (1998), and details on the procedure can be found in the Supplementary Publication. UV-laser ablation was performed by rastering the focused beam of a frequency-quadrupled Nd-Yag laser to produce ablation pits with a dimension of at least 50 × 50 × 50 μm. *In situ* Ar-ion laser fusion was accomplished by firing approximately five, 500 ms bursts of a focused Ar-ion laser at a power level of 2.8 W to produce roughly 100 μm diameter melt pits. Total fusion of individual grains was carried out by expanding the Ar-ion laser beam to a width of >2 mm. Incremental heating took place in a double-vacuum resistance furnace controlled to within c. 5 K.

Analytical blanks during furnace experiments varied as a function of temperature, but were typically in the range of 10^{-15}–10^{-16} moles at M/e 40. Analytical blanks during laser experiments, monitored after every ten analyses, were less than 5×10^{-16} moles at M/e 40. All isotopic measurements were corrected for system blanks, neutron-induced interference, and mass fractionation before apparent age calculations. We report three types of apparent ages. Plateau ages, with uncertainties of 2σ, are quoted when an appropriate fraction of the gas extracted during FSH-experiments fit the criteria for a plateau as suggested by Fleck *et al.* (1977). Isochron ages, also reported at 2σ, are reported when the extracted gas define an isochron on a plot of $^{36}Ar/^{40}Ar$ *v.* $^{39}Ar/^{40}Ar$ based on the MSWD parameter (Wendt & Carl 1991). In most cases, however, the radiogenic yields of our laser experiments were so high that the data were too clustered on such diagrams to define robust isochrons. For these experiments, we simply quote the mean apparent date. We detected no systematic apparent age variations across single mica grains dated by laser, and there was no significant variation in the laser-ages of different aliquots of a single mica, suggesting that all analysed mica samples were homogeneous in $^{40}Ar/^{39}Ar$. As a consequence, we quote two satndard errors of the mean as the uncertainty for mean apparent ages. The uncertainties for all apparent ages include propagated contributions for analytical errors, blank errors, and errors in the J-value.

inherited. The monazite crystals range from reversely discordant to within error of concordant to slightly normally discordant with $^{207}Pb/^{235}U$ dates ranging from 429 to 403 Ma. We speculate that this spread in $^{207}Pb/^{235}U$ dates may record the timespan of high-temperature metamorphic processes associated with *in-situ* anatectic melting of the gneissic hostrock and the segregation of melt into veins. The four xenotime crystals analysed are normally discordant and fall along a linear array (MSWD=0.98) with an upper intercept of 430 ± 6.5 Ma. On the basis of these it is difficult to determine a crystallization age for the leucocratic vein; however, the upper intercept age of the xenotime regression we interpret as a good estimate of this age. A large muscovite crystal from the same granite sample (96-60) was dated by $^{40}Ar/^{39}Ar$ laser spot fusion. A considerable but unsystematic variation in dates (*c.* 429–396 Ma) between spots throughout the grain was observed. The sample data yield an inverse isochron date of 405.1 ± 9.8 Ma (Fig. 9b). The variation in spot data can, to some degree, be explained by the large uncertainties (5–15 Ma) due to extraction of small volumes of gas. However, some of the age variation may record a real uneven distribution of radiogenic argon. Muscovite crystals from the gneiss (95, 10/8-3) cut by the granites were dated by laser total fusion, yielding a weighted average of 397.1 ± 2.8 Ma.

Peraluminous granite cutting F_2 folds at Kap Lapparent. Peraluminous granite and pegmatite veins up to *c.* 20 m thick cut the F_2 folds in the gneisses at Kap Lapparent (Fig. 4d). A granitic vein in the western section of the outcrop face was sampled for $^{40}Ar/^{39}Ar$ dating (96-58). Fifteen Ar-ion laser spots in a large muscovite crystal give dates ranging from 387 Ma to 359 Ma, and an inverse isochron date of 378.7 ± 5.7 Ma (Table 2; Fig. 10a). Total fusion of fragments of a large muscovite grain gave a weighted average date of 380.8 ± 2.7 Ma. Ar-ion laser spots in a large biotite grain yielded an inverse isochron date 390.2 ± 8.7 Ma (Fig. 10b). In addition, a single large biotite grain was analysed by furnace step heating, giving a near-plateau age of 386.9 ± 1.5 Ma (Fig. 10c and d). Because muscovite has a higher closure temperature for ^{40}Ar loss than biotite (McDougall & Harrison 1988), the older biotite $^{40}Ar/^{39}Ar$ date suggests contamination with excess ^{40}Ar in the biotite.

Discussion

The structural and isotopic data indicate that peraluminous granites were emplaced into the Fjord Region Detachment Zone and subsequently cooled and/or deformed over a period

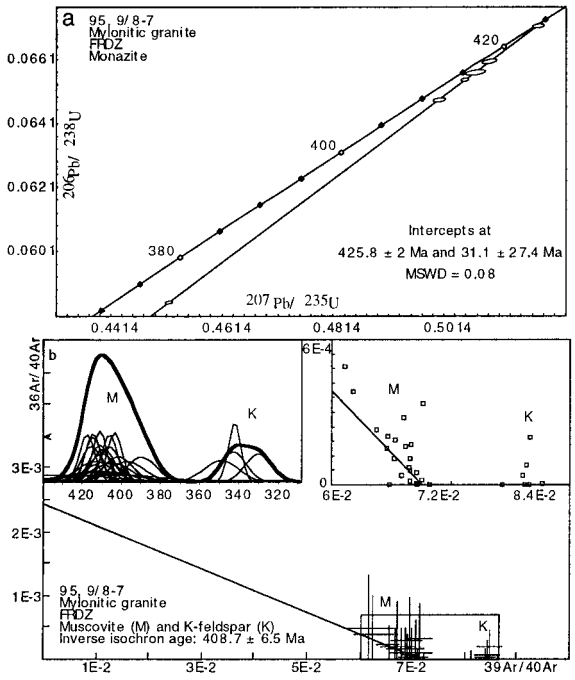

Fig. 7. Isotope data from the mylonitic granite at the top of Fjord Region Detachment Zone. (**a**) Concordia diagram of two discordant monazites in from the uppermost detachment zone. The analyses define a linear array with an upper intercept of 425.8 ± 2.0 Ma (MSWD=0.08). (**b**) Inverse isochron plot of laser spot fusion data from thin section. Ages from the muscovite ('M') and K-feldspar ('K') clearly plot apart, as demonstrated in the graph showing the ages with error plotted as gausian distributions. The heavy line marks the sum of individual spots plotted below with thin lines. The other insert shows the inverse isochron line produced from the muscovite data. Initial $^{36}Ar/^{40}Ar$ ratio is 412 ± 123. The inverse isochron age of 408.7 ± 6.5 compares well to the error weighted average age.

of more than 80 Ma. Kinematic data link the tectonic evolution to exhumation of the central metamorphic core complex, through tectonic thinning of the crust. The evolution of the footwall at Kejser Franz Joseph Fjord can be divided into three stages: (1) formation of the Niggli Spids migmatites in a metamorphic core complex, partly coeval with anatexis and (2) development of the Fjord Region Detachment Zone as a major extensional shear zone along the eastern border of the complex; and (3) cooling through the closure temperature for Ar-diffusion in muscovite during early Devonian and in K-feldspar in the Carboniferous.

Niggli Spids Migmatite Dome

The peraluminous granites dated in the study area are interpreted to have been sourced from migmatites in the carapace of Niggli Spids Migmatite Dome. These leucocratic melts segregated upward into granitic veins that cut folded paragneisses and are themselves variably deformed. Peraluminous granites become increasingly deformed at higher structural levels as the Fjord Region Detachment Zone is approached, and similar granites also intrude the lowermost Eleonore Bay Supergroup in the hanging wall directly north of Kejser Franz Joseph Fjord. The metasediments below the Fjord Region Detachment Zone have been alternately interpreted to be either Late Proterozoic (Eleonore Bay Supergroup) (Haller 1953) or Mid-Proterozoic (e.g. Henriksen 1985; Leslie & Higgins 1998) in age (Fig. 2). Precambrian Rb–Sr and U–Pb zircon dates from peraluminous granties in the same region have been interpreted as evidence for a Grenvillian synorogenic granites (Rex & Gledhill 1981; Leslie & Higgins 1998). The field relationships and U–Pb data presented here indicate that both the metamorphism and the peraluminous granites studied here are Caledonian, and we therefore suggest that the *c.* 1 Ga granites are rift-related anorogenic intrusions.

A late to post metamorphic granite at Junctiondal is estimated to be 430 ± 6.5 Ma (Fig. 3). We interpret the age of the mylonitic granite in the detachment zone not to be younger than 425.8 ± 2 Ma. The age data and the eastward increase in brittle fabrics suggest that the eastward and structurally upward increase in strain of the granites reflects upward-narrowing of the detachment zone with time, rather than differences in intrusive ages. Our work therefore supports Haller's (1953, 1971) interpretation that the metamorphism and peraluminous granites above the Niggli Spids Migmatite Dome are Caledonian, and contrasts interpretations of Leslie & Higgins (1998), who, based on *c.* 1000 Ma Rb–Sr ages for leucogranites in the same area (Rex & Gledhill 1981), named the footwall of the detachment the 'Greenville triangle'.

The thin veins of peraluminous granites are interpreted to be derived by anatectic melting in the micaceous layers. Vold (1997) has reported nearly isothermal decompression of the migmatite dome in Kempes Fjord (Fig. 1), under *P–T* conditions that would cause anatexis in micaceous rocks (England & Thompson 1986). None of the peraluminous granites cut across the detachment zone into the Eleonore Bay Supergroup in Kejser Franz Joseph Fjord, but leucogranites are common in the hanging wall farther north (Koch & Haller 1971), which is consistent with the interpretation that displacement across the detachment partly post-dates emplacement of the granites.

East–west-trending F_1 folds and north–south-trending F_2 and F_3 folds are recorded in this study. Similar fold directions dominate the structurally deeper infrastructure (Haller 1971), and are in general agreement with observations by Hartz & Andresen (1995). Leslie & Higgings (1998) described four deformational phases in the same region. They suggest that oblate flattening (D_1), progressively developing into the penetrative and regional syn-magmatic D_2 structures including gently ESE-plunging lineations and associated east-verging asymmetric folds, and east-verging crenulation folds (D_3), followed by north–south-oriented open folds (D_4). These observations are also in general agreement with the observations presented here, although we choose to group D_2 and D_3 into one fold phase (our F_2). However, in contrast to Leslie & Higgins (1998), we suggest that the east-verging (F_2) folds at the base of the Eleonore Bay Supergroup are best explained by top-to-the-east extensional faulting, rather than top-to-the-NW thrusting and suggest that the extensional structures cut thrust related structures. The F_1 folds and microstructures in the lineated gneisses record top-to-the-east extensional displacement, east–west elongation and north–south shortening, in the section we studied. Deeper in the section are the F_1, structures associated with top-to-the-NW thrusting. These structures are interpreted to have formed during the earliest syncontractional unroofing of the suprastructure along the detachment zone. Similar structures can be found in the orogen transverse folds of the Scandinavian Caledonides, which can be explained by constrictional strain resulting from variations in forces between the colliding continents and gravity (Chauvet & Seranne 1994; Hartz & Andresen 1997).

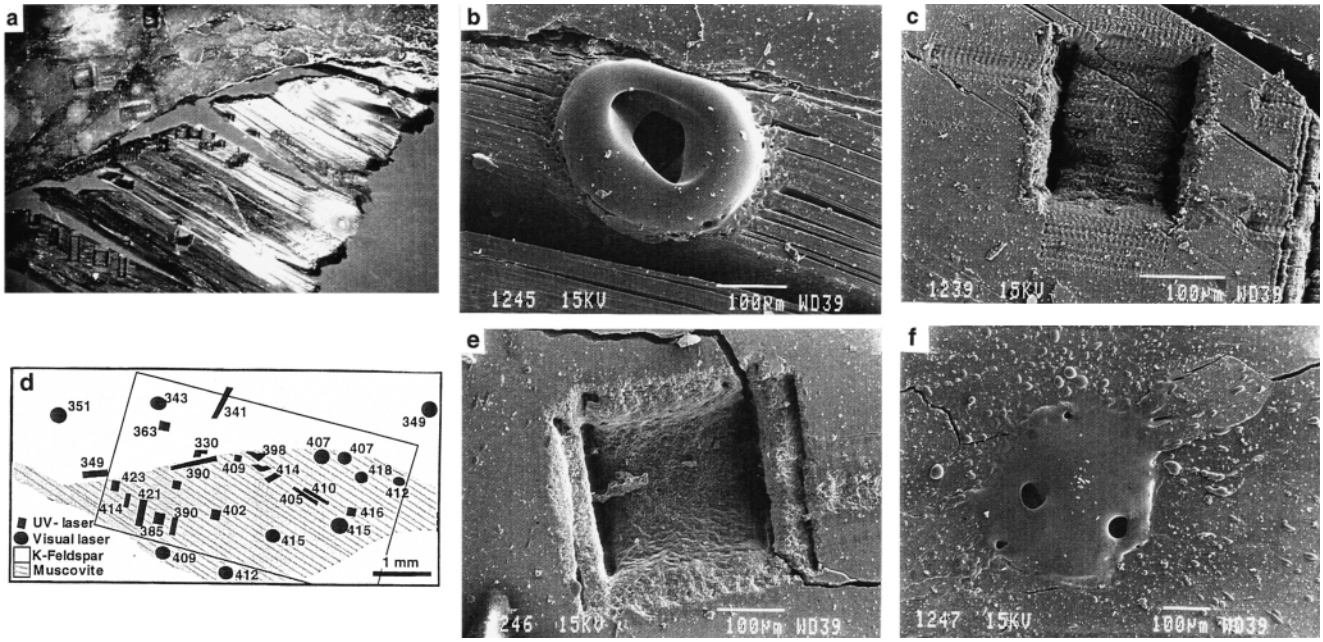

Fig. 8. Photomicrographs and drawings of feldspar and muscovite in thin sections of mylonitic granite at the top of Fjord Region Detachment Zone (95, 9/8-7). (**a**) Spots were first fused with the UV laser (square pits) and then the Ar-ion laser (melt holes), which caused the damage to the sample. Notice how the round spots fired by the Ar-ion laser are surrounded by large white damage zones, and material surrounding the square UV spot is virtually undeformed. (**b**) Spot in muscovite melted by the Ar-ion laser. Notice how the muscovite split along foliation away from the spot. (**c**) The spot milled into a muscovite with the UV-laser is of about the same size, but shows little damage to surrounding material. The UV-tracks outside the pit result from late night fumbling with the laser control device. The box milled out by the UV-laser is considerably larger than the melt spot formed by the two blasts with the Ar-ion laser. Nevertheless the UV spot yielded only 1/3 to 1/2 as much ^{39}Ar as the Ar-ion laser spot, which indicate that not all of the argon gas were extracted from the material ablated by the UV-laser. (**d**). Sketch of the thin section showing spot ages (in Ma) within both muscovite and K-feldspar. The frame marks the position of the photo in (a). (**e**) K-feldspar dated by the UV-laser have nice square pits with little damage outside the pit. (**f**) The spot dated by two blasts of the Ar-ion laser shows a large area with damage, and extrusion of melted material.

The age of the large-wavelength north–south-trending F_3 folds structures is enigmatic. Similar style folds occur in the Devonian collapse basins directly east of the detachment, suggesting that F_3 folds may partly be late Palaeozoic, and unrelated to main Caledonian orogenic event.

Fjord Region Detachment Zone

The structural style of the Fjord Region Detachment Zone is typical of detachment zones in displaying a progression from ductile to brittle deformation, and a narrowing of the shear zone at higher structural levels (e.g. Davis 1983). There is a gradual transition between the non-mylonitic rocks at the Niggli Spids Migmatite Dome and the *c.* 300 m of thick, mylonitic, top-to-the-east extensional detachment zone above, and a dramatic upward decrease in metamorphic grade across the brittle Late Brittle Detachment Fault. Kinematic indicators in the lowermost part of the hanging wall show top-to-the-east extensional shearing, related to the hanging-wall cut-off. Zones of brittle deformation also affect deeper crustal rocks, consistent with uplift of the deeper part of the section by brittle faulting.

Taken together, the U–Pb data and the oldest muscovite cooling ages support emplacement of the syn-tectonic granites around 430–425 Ma, requiring initiation of movement on the Fjord Region Detachment Zone at about the same time. Large muscovites from the upper part of the detachment zone yield $^{40}Ar/^{39}Ar$ dates of 409–408 Ma, and smaller muscovites from the same samples are slightly younger (*c.* 404 Ma). Eight metres structurally below the Late Brittle Detachment Fault, small muscovites yield dates of *c.* 400 Ma and at Junctiondal muscovite yield dates of *c.* 397 Ma. $^{40}Ar/^{39}Ar$ dates of large muscovites and biotites range from *c.* 386 to *c.* 376 Ma at Kap Lapparent (Table 2). These data document that the structurally deepest rocks were the last to cool below the retention temperature for Argon, with a maximum difference of 25 Ma between large micas in the top of the detachment zone and those at Kap Lapparent at deeper structural levels (Table 2). This progression of timing could be relate to movement on shear zones below the sampled rocks at Junctiondal (Fig. 3) or could be due to thermal relaxation of the uplifted core complex.

The feldspar dates of *c.* 349 Ma for the mylonites in the detachment are distinctly younger than feldspars in leucogranites above the Fjord Region Detachment Zone (*c.* 408 Ma; Hartz 1998). This effect may either reflect the reduced grain size in the mylonites, but may suggest that the footwall rocks could have been uplifted from deeper levels of the crust and cooled later than the hanging-wall rocks. Micas in the hanging wall closed between *c.* 419 and *c.* 413 Ma (Hartz 1998), indicating that initial cooling of the lowermost hanging and uppermost footwall of the Fjord Region Detachment Zone was nearly synchronous. The data from the footwall of the detachment zone, therefore, not only express the level of uplift but also record slow cooling from the high *T*/low *P* conditions recorded by Vold (1997). The delay in cooling, therefore, is consistent with an elevated heat flux in the core complex lasting well into the Carboniferous period; however more

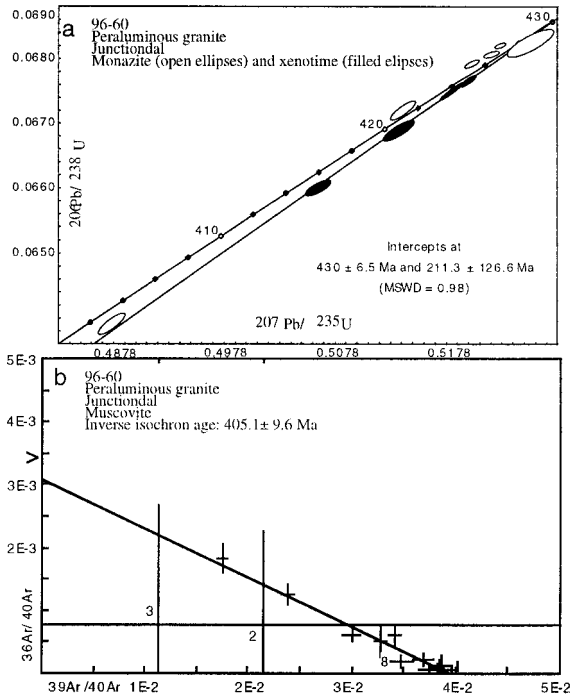

Fig. 9. Isotope data from granitic vein at Junctiondal. (**a**) Concordia diagram, showing ages of single monazites (m) and a xenotime (x). The four xenotime crystals analysed are normally discordant and fall along a linear array (MSWD=0.98) with an upper intercept of 430 ± 6.5 Ma. The oldest monazite is interpreted as inherited, and the youngest is interpreted to be reset by lead-loss. (**b**) Typical inverse isochron plot of a mica dated by spot fusion. Some spots (2 and 3) give little gas, causing large errors. Other spots show contamination with air, yielding a 'near' inverse isochron line. The inverse isochron age compares to the error-weighted mean age, but shows a much larger error. Spot '8' plots below the isochron suggesting that the old age (*c*. 429 Ma) results from excess argon. Initial $^{36}Ar/^{40}Ar = 324.3 \pm 40.3$, age = 405.1 ± 9.8 Ma.

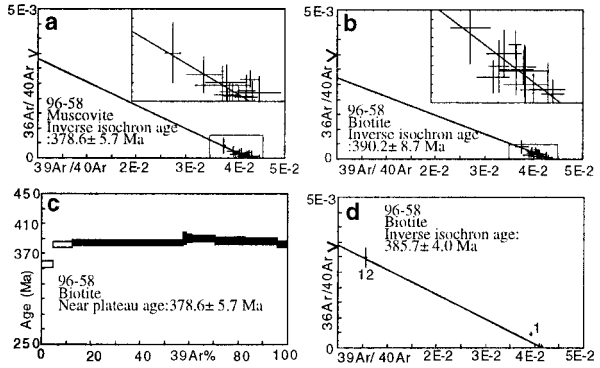

Fig. 10. Isotope data from a granite vein at Kap Lapparent. (**a**) Inverse isochron plot of a large muscovite dated by Ar-ion laser spot fusion. Initial $^{36}Ar/^{40}Ar = 300.2 \pm 83.9$, age = 378.6 ± 5.7 Ma. (**b**) Inverse isochron plot of a large biotite dated by Ar-ion laser spot fusion. Initial $^{36}Ar/^{40}Ar = 366.76 \pm 84.6$, age = 390.2 ± 8.7 Ma. (**c**) Age spectra produced by furnace step heating of biotite. Near plateau age 386.9 ± 1.5 Ma. Steps 3–11 (shaded) equals 87.3% ^{39}Ar. There is therefore not a plateau *senso-stricto*, although the total gas age of these steeps is interpreted as reliable. (**d**) Inverse isochron plot from biotite. The sample is highly radiogenic, and the inverse isochron age compares closely to the plateau age. Spot 1 is not included. Initial $^{36}Ar/^{40}Ar = 295.7 \pm 44.2$, age = 385.7 ± 4.0 Ma.

K-feldspar analysis is needed to fully evaluate the low temperature evolution of the orogen, and the effect of the contractional event registered in the collapse basins are not well constrained.

Regional implications

An extensive mapping and isotopic dating project by the Geological Survey of Greenland recently has resulted in a series of papers on the infrastructure–suprastructure boundary in the Ardencaple fjord area (Fig. 1). Two different tectonic models have resulted from these studies. Soper & Higgins (1993) suggest that the zone is a Vendian detachment reactivated by Caledonian thrusting. Dallmeyer *et al.* (1994), Strachan (1994), and Friderichsen *et al.* (1994) conclude that the structure is a Late Silurian to Early Devonian detachment, reactivated by minor Early through Middle Devonian thrusting.

Dallmeyer *et al.* (1994) present numerous $^{40}Ar/^{39}Ar$ dates above and below 'thrusts and low angle shear zones' separating the Eleonore Bay Supergroup from the underlying basement gneisses. Muscovite dates in the hanging wall of the shear zone range between *c*. 422 and 411 Ma, whereas muscovite dates in the footwall range from *c*. 402 to 380 Ma. Muscovites from a major lateral shear zone in the footwall yield dates mostly between *c*. 380 and 375 Ma. These Early Devonian ages were interpreted to date 'metamorphism, thrusting, strike-slip shear zones and regional folding' (Dallmeyer *et al.* 1994). We suggest that Early Devonian ages in the footwall rocks relate to delayed cooling, rather than to a separate phase of metamorphism.

Extensional uplift was ongoing by 430–425 Ma (Early Silurian) when the granites below the Fjord Region Detachment Zone formed. Thrusting in the foreland of the East Greenland Caledonides is argued to have continued until 399 Ma (Dallmeyer *et al.* 1994). Across the orogen in the Scandinavian Caledonides thrusting continued at least until Late Silurian (Roberts & Gee 1985; Northrup 1997). Collectively these data imply that extension in the East Greenland Caledonides initiated while plate convergence was still ongoing.

Conclusions

Structural and isotopic data from the high strain zone at Kejser Franz Joseph Fjord indicate that it is a long-lived extensional shear zone developed under decreasing *P–T* conditions. Its extensional history, initiated by *c*. 430–425 Ma in an overall top-to-the-NW contractional setting and we speculate that the near-isothermal uplift documented below the Fjord Region Detachment Zone farther south caused decompressional anatexis. Our isotopic results indicate that the dated synkinematic anatectic granites are Caledonian rather than Grenvillian in age. Niggli Spids Migmatite Dome therefore is a Caledonian feature intruded earlier by *c.* 1 Ga anorogenic granites. This tectonic scenario is similar to Haller's (1953) model for formation of the domes as Precambrian crystalline rocks 'rejuvenated' during the Caledonian orogeny. Our results conflict with more recent models, which suggest that the footwall of the Fjord Region Detachment Zone is only weakly 'Caledonized'.

Ductile strain progressively increases upward in the Fjord Region Detachment Zone. Subsequent semibrittle-to-brittle deformation and cooling of the footwall rocks is recorded in the mylonites, gneisses and granites. The transition from ductile to semi-brittle to brittle behavior is also reflected in by the $^{40}Ar/^{39}Ar$ muscovite-data that record cooling at *c*. 407 Ma in the upper part of the detachment zone to *c*. 375 Ma in the lowest part of the studied transect. Cooling is recorded in K-feldspar which closed to Ar-diffusion at *c*. 349 Ma.

In conclusion, we suggest that the overall tectonic framework of rocks in the study area can be attributed to syn-collisional Silurian to Devonian gravitational collapse, and subsequent thermal relaxation.

M. Lynn, G. Bye-Fjell and T. Winje are thanked for assistance in preparation of the special thin sections, and mineral separation. W. Hames is thanked for instructing E.H.H. in mineral separation and B. Olszewski is thanked for patiently introducing E.H.H. to the MIT Argon lab facilities. We thank the Danish Polar Centre, and Sirius (the Danish military dog-sled patrol) for logistical assistance. The photo in Fig. 4d was taken by J. Vold. The paper benefited greatly from comments from E. Eide and reviewers M. G. Stelthenpohl and S.P. Kelley. E.H.H. thanks P. Hoffman for inviting him to spend his sabbatical at Harvard University, where this paper was completed. Fieldwork was sponsored by Nansen fondet, Norges Forskningsråd and VISTA.

References

Andersen, T.B. 1993. The role of extensional tectonics in the Caledonides of south Norway: Discussion. *Journal of Structural Geology*, **15,** 1379–1380.

Andresen, A., Hames, W.E. & Hartz, E. 1995. New constraints on timing and nature of orogenic deformation within the East Greenland Caledonides. *Geological Society of America, Abstracts with Programs*, **27,** 6.

——, Hartz, E. & Vold, J. 1998. A late orogenic extensional origin for the infracrustal gneiss domes of the East Greenland Caledonides (72°–74°N). *Tectonophysics*, **285,** 353–369.

Berthé, D., Choukroune, P. & Jegouzo, P. 1979. Orthogneiss, mylonite and non-coaxial deformation of granites: the example of the South Armorican shear zone. *Journal of Structural Geology*, **1,** 31–42.

Brueckner, H.K., Gilotti, J.A. & Nutman, A. 1998. Caledonian Eclogite-facies metamorphism of Early Proterozoic protoliths from the North-East Greenland eclogite Province. *Contributions to Mineralogy and Petrology*, **130,** 103–120.

Burchfiel, B. & Royden, L.H. 1985. North-South extension within the convergent Himalayan region. *Geology*, **13,** 679–682.

Burg, J.P., Guiraud, M., Chen, G.M. & Li, C.G. 1984. Himalayan metamorphism and deformation in the North Himalayan belt (South Tibet, China). *Earth and Planetary Science Letters*, **00,** 391–400.

Chauvet, A. & Seranne, M. 1994. Extension-parallel folding in the Scandinavian Caledonides: Implications for late orogenic processes. *Tectonophysics*, **238,** 31–54.

Dallmeyer, R.D., Strachan, R.A. & Henriksen, N. 1994. $^{40}Ar/^{39}Ar$ mineral age record in NE Greenland: implications for tectonic evolution of the North Atlantic Caledonides. *Journal of the Geological Society, London*, **151,** 615–628.

Davis, G.H. 1983. Shear-zone model for the origin of metamorphic core complexes. *Geology*, **11,** 342–347.

Dennis, A.J. & Secor, D.T. 1987. A model for the development of crenulations in shear zones with applications from southern Appalachian piedmont. *Journal of Structural Geology*, **9,** 809–817.

England, P. & Thompson, A. 1986. Some thermal and tectonic models for crustal melting in continental collision zones. *In*: Coward, M.P. & Ries, A.C. (eds) *Collision Tectonics.* Geological Society, London, Special Publications, **19,** 83–94.

Escher, J. & Jones, K.A. 1998. Caledonian thrusting and extension in Frœnkl Land, East Greenland (73°–73°30′N): Preliminary results. *Danmarks og Grønlands Geologiske Undersøkelse Rapport*, **28,** 29–42.

Fleck, R.J., Sutter, J.F. & Elliot, D.H. 1977. Interpretation of discordant $^{40}Ar/^{39}Ar$ age spectra of Mesozoic tholeiites from Antarctica. *Geochimica et Cosmochimica Acta*, **41,** 15–32.

Fränkl, E. 1956. Some general remarks on the Caledonian chain of East Greenland. Meddelelser om Grønland, **206**.

Friderichsen, J.D., Strachan, R.A. & Henriksen, N. 1994. Basement-cover relationships and regional structure in the Grandjean Fjord-Bessel Fjord region 72°–76°N, North-East Greenland. *Rapport Grønlands Geologiske Undersøgelse*, **162,** 17–33.

Haller, J. 1953. *Geologie und Petrographie von West-Andree's Land und Öst-Fränkls Land (Nord-öst Grönland)*. Meddelelser om Grønland, **113**.

—— 1955. Der *'Zentrale Metamorphe Komplex' von Nordöstgrönland. Teil I. Die geologiske Karte von Suess Land, Gletscherland und Goodennoughs Land*. Meddelelser om Grønland, **73**.

—— 1970. *Tectonic map of East Greenland (1:500,000)*. Meddelelser om Grønland, **171**.

—— 1971. *Geology of the East Greenland Caledonides*. New York, Interscience Publishers.

Hartz, E.H. 1998. *Late orogenic evolution of the East Greenland and Scandinavian Caledonides*. Dr Scient thesis, University of Oslo.

—— & Andresen, A. 1995. Caledonian sole thrust of central east Greenland: A crustal-scale Devonian extensional detachment? *Geology*, **23,** 7, 637–640.

—— & —— 1997. From collision to collapse: Complex strain permutations in the hinterland of the Scandinavian Caledonides. *Journal of Geophysical Research*, **102,** B11, 24 697–24 711.

——, ——, Martins, M.W. & Hodges, K.V. Timing of syn-collisional exhumation of deep crustal rocks in the East Greenland Caledonides. *Tectonics*, in press.

——, Torsvik, T.H. & Andresen, A. 1997. Carboniferous age for the East Greenland 'Devonian' basin: Paleomagnetic and isotopic constraints on age, stratigraphy, and plate reconstructions. *Geology*, **25,** 675–678.

Henriksen, N. 1985. The Caledonides of central East Greenland 70°–76°N. *In*: Gee, D.G. & Sturt, B.A. (eds) *The Caledonide orogen, Scandinavia and related areas*. John Wiley & Sons Ltd, London, 1095–1013.

Higgins, A.K. 1976. Pre-Caledonian metamorphic complexes within the southern part of the East Greenland Caledonides. *Journal of the Geological Society, London*, **132,** 289–305.

Hodges, K.V. 1998. $^{40}Ar/^{39}Ar$ geochronology using the laser microprobe. *In*: McKibben, M.A. & Shanks, W.C. (eds) *Reviews in Economic Geology 7: Applications of Microanalytical Techniques to Understanding Mineralizing Processes*, Society of Economic Geologists, Tuscaloosa, AL, 53–72.

—— & Bowring, S.A. 1995. $^{40}Ar/^{39}Ar$ thermochronology of isotopically zoned micas: Insights from the southwestern USA Proterozoic orogen. *Geochimica et Cosmochimica Acta*, **59,** 3205–3220.

Koch, L. & Haller, J. 1971. *Geological map of East Greenland 72°–76°N*. Meddelelser om Grønland, **183**.

Krogh, T.E. 1973. A low contamination method for hydrothermal decomposition of zircon and extraction of U and Pb for isotopic age determination. *Journal?*, **37,** 488–494.

Larsen, P.H. & Bengaard, H.J. 1991. The Devonian basin initiation in East Greenland: a result of sinestral wrench faulting and Caledonian extensional collapse. *Journal of the Geological Society London*, **148,** 355–368.

Leslie, A.G. & Higgins, A.K. 1998. On the Caledonian geology of Andreé Land, Eleonore Sø and adjacent nunataks (73°–74°N), East Greenland. *Danmarks og Grønlands Geologiske Undersøkelse Rapport*, **28,** 11–28.

Ludwig, K.R. 1989. *Pb. dat: A computer program for processing raw Pb-U-Th isotopic data*. US Geological Survey Open-file report.

—— 1990. *Isoplot: A plotting and regression program for radiogenic-isotope data*. US Geological Survey Open-file report.

McDougall, I. & Harrison, T.M. 1988. *Geochronology and thermochronology by the $^{40}Ar/^{39}Ar$ method.* Oxford University Press, New York.

Nathorst, A.G. 1901. Bidrag til nordøst Grønlands geologi. *Geologisk Förening Stockholm Förhandlinger*, **23,** 207, 275–306.

Northrup, C.J. 1997. Timing structural assembly, metamorphism, and cooling of Caledonian Nappes in the Ofoten-Efjorden area, North Norway: Tectonic insights from U-Pb and $^{40}Ar/^{39}Ar$ geochronology. *Journal of Geology*, **105,** 565–582.

Onstott, T.C., Phillips, D. & Pringle-Goodell, L. 1991. Laser microprobe measurements of chlorine and argon zonation in biotite. *Chemical Geology*, **90,** 145–168.

Rex, D. & Gledhill, A.R. 1981. Isotopic studies in the East Greenland Caledonides (72–74°N)—Precambrian and Caledonian ages. *Geological Survey of Greenland, Report*, **104,** 47–72.

—— & Higgins, A.K. 1985. Potassium-argon mineral ages from the East Greenland Caledonides between 72° and 74°N. *In*: Gee, D.G. & Sturt, B.A. (eds) *The Caledonide orogen, Scandinavia and related areas*. John Wiley & Sons Ltd, London, 1115–1124.

——, Gledhill, A.R. & Higgins, A.K. 1977. Precambrian Rb-Sr isochron ages from the crystalline complexes of inner Forsblad Fjord, East Greenland. *Bulletin Grønlands Geologisk Undersøgelse*, **80,** 127–133.

Roberts, D. & Gee, D.G. 1985. An introduction to the structure of the Scandinavian Caledonides. *In*: Gee, D.G. & Sturt, B.A. (eds). *The Caledonide orogen, Scandinavia and related areas*. John Wiley & Sons Ltd, London. 485–497.

Samson, S.D. & Alexander, E. 1987. Calibration of the interlaboratory $^{40}Ar/^{39}Ar$ dating standard, MMhb-1. *Chemical Geology (Isotope Geosciences Section)*, **66,** 27–34.

Stacey, J.S. & Kramers, J.D. 1975. Approximation of terrestial lead isotopes evolution by a two-stage model. *Earth and Planetary Science Letters*, **26,** 207–221.

Steiger, R.H. & Jäger, E. 1977. Subcommission on geochronology; convention on the use of decay constants in geo- and cosmochronology. *Earth and Planetary Science Letters*, **36,** 359–362.

Sønderholm, M. & Tirsgaard, H. 1993. Lithostratigraphic framework of the upper Proterozoic Eleonore Bay Supergroup of East and North Greenland. *Bulletin Grønlands Geologiske Undersøgelse*, **167,** 38.

Soper, N.J. & Higgins, A.K. 1993. Basement-cover relationships in the East Greenland Caledonides: evidence from the Eleonora Bay Supergroup at Ardencaple Fjord. *Transactions of the Royal Society of Edinburgh*, **84,** 103–115.

Strachan, R.A. 1994. Evidence in North-East Greenland for Late Silurian-Early Devonian regional extension during the Caledonian Orogeny. *Geology*, **22,** 913–916.

Vold, J. 1997. *Et studie av den tektonometamorfe utvikling av gneisene i liggblokken til 'the Fjord Region Detachment Zone' på Kap Hedlund, Sentrale Øst Grønland*. Cand. Scient, University of Oslo.

Wegmann, C.A.E. 1935. *Preliminary report on the Caledonian orogeny in Christian X's Land (North-East Greenland)*. Meddelelser om Grønland, **103**.

Wendt, I. & Carl, C. 1991. The statistical distribution of the mean squared weighted deviation. *Chemical Geology*, **86,** 275–285.

Whittard, W.F. 1930. Geology, appendix II. *In*: Wordie, J.M. (ed.) *Cambridge East Greenland Expedition, 1929, Ascent of Petermann Peak*. *Geographical Journal,* **75,** 495–497.

Received 20 November 1998; revised typescript accepted 12 January 2000.
Scientific editing by Ray Burgess.